Pressure-Induced Hydrogen Transfer in 2-Butyne via a Double CH···π Aromatic Transition State

Peijie Zhang,[1,▽] Xingyu Tang,[1,▽] Chunfang Zhang,[2] Dexiang Gao,[1] Xuan Wang,[1] Yajie Wang,[1] Wenhan Guo,[3] Ruqiang Zou,[4] Yehua Han,[5] Xiaohuan Lin,[1] Xiao Dong,[6] Kuo Li,[1] Haiyan Zheng,[1,] Ho-kwang Mao[1]*

[1]Center for High Pressure Science and Technology Advanced Research, Beijing, 100094, P. R. China.

[2]College of Chemistry and Environmental Science, Hebei University, Baoding, 071002, P. R. China.

[3]Great Bay University, Dongguan, 523000, P. R. China.

[4]School of Materials Science and Engineering, Peking University, Beijing, 100871, P. R. China.

[5]State Key Laboratory of Heavy Oil Processing, College of Chemical Engineering and Environment, China University of Petroleum-Beijing, Beijing, 102249, P. R. China.

[6]Key Laboratory of Weak-Light Nonlinear Photonics, School of Physics, Nankai University, Tianjin, 300071, P. R. China.

[▽]P.Z. and X.T. contributed equally.

Corresponding Author: Haiyan Zheng Email: zhenghy@hpstar.ac.cn

Table of Contents

S1. Experimental procedures and calculation details

S1.1 In situ high-pressure Raman, IR, and X-ray diffraction experiments

2-Butyne (C_4H_6, 99.9%) was purchased from J&K Scientific Ltd and used without further purification. Our Raman and IR spectra as well as X-ray diffraction (XRD) were measured using a symmetric diamond anvil cell (DAC). Type-II diamond anvils were used for IR experiment to avoid absorption band at 1000-1300 cm^{-1}. All diamonds were polished to a culet diameter of 300 μm. T301 stainless steel gaskets were pre-indented to a thickness of ~30 μm and holes with d = 150 μm were drilled at the center of the indentation to serve as the sample chamber. In order to avoid the sample volatilization and possible big grains or preferred orientation, the whole DAC was cooled in liquid nitrogen environment firstly and sample (liquid) was frozen on the cold gasket, and then the DAC was sealed at low temperature. The pressure was determined by measuring the ruby fluorescence, according to the equation P (GPa) = 248.4[(λ/ λ_0)7.665 - 1].[1] Raman experiments were carried out on a Renishaw Raman microscope with 532 nm laser line from a Nd:YAG laser source. The system was calibrated by the Raman peak of Si. IR experiments were performed on a Bruker VERTEX 70v with HYPERION 2000 microscope. The spectra were collected in transmission mode in the range of 600-4000 cm^{-1} with a resolution of 4 cm^{-1} through a 20 × 20 μm^2 aperture. The synchrotron XRD data were collected at beamline 16 ID-B, Advanced Photon Source (APS), Argonne National Laboratory. The monochromated incident X-ray

wavelength is 0.4340 Å. The preliminary data reduction was performed by using the Dioptas program.[2] Rietveld refinement was performed for XRD data by using Jana 2006 software.[3]

S1.2 Synthesis of sample PE-20

The sample PE-20 was synthesized using a VX3 Paris-Edinburgh press (PE Press) equipped with double-toroid sintered diamond anvils, with a sample volume of 16.8 mm^3. The liquid 2-butyne was dropped into an encapsulated stainless-steel gasket under liquid N_2 temperature and frozen immediately. After the gasket was fully filled, the whole gasket sets containing the sample were moved into the VX3 PE press and the cell was closed in a few seconds. An automatic hydraulic oil syringe pump drove the system and the pressure was estimated from the Edinburgh group calibration curve.[4] In order to avoid sample leakage, the oil pressure was quickly increased up to 150 bar, about 1.5 GPa on the sample. Then the sample was compressed to about 20 GPa (oil pressure 1600 bar). The sample were kept under target pressure for about 12 hours. After releasing the pressure, white powder was obtained. The rates of the compression were as follows: 4 bar/min from 150 bar to 400 bar, 2 bar/min from 400 bar to 800 bar and 1 bar/min from 800 bar to target oil pressure. The gaskets were removed in the glovebox and colorless solid sample was obtained.

S1.3 High-pressure single crystal X-ray diffraction experiment

The single crystal X-ray diffraction (XRD) data was collected on an XtaLab Pro X-ray Single Crystal Diffractometer with Mo K_α X-ray source and HPAD detector. The DAC was loaded on a specific goniometer head. To avoid the influence of the diamond and gasket, diffraction points with intensity higher than 10000 and the diffraction ring around 2.03 Å which belong to the diffraction of iron (gasket) were deleted before indexing.

S1.4 High-Resolution Gas Chromatography Mass spectrometry experiment

The obtained sample PE-20 was dissolved in 0.5 mL n-hexane ($C_{16}H_{14}$, HPLC purity, 99.9%, J. T. Baker). The extracted portion was measured by the High-Resolution Gas Chromatography Mass spectrometry (GC-MS). 1 uL sample was injected automatically in the splitless mode at 280 ºC. The GC oven was increased from 40 ºC (held for 2 mins) to 280ºC (held for 5 mins) at a rate of 5 ºC/min. The temperature of the transfer lines and ion source were both set at 280 ºC. The system was operated with an electron ionization source (EI) at 70 eV. Scan spectra were recorded in the

range of 50-750 m/z using the full scan mode at 60k resolving power (FWHM at m/z 200) mass resolution. The chemical ionization (CI) source was also utilized in the measurement of the sample PE-20 for identification of the molecular formula. The positive chemical ion mode was applied and methane (99.999%, Beijing AP BAIF Gases Industry Co., Ltd) was used as reagent gas at a flow rate of 1.5 mL/min with a source temperature of 280 ºC. The EI and CI of n-hexane were also measured by the same procedure as stated above to act as a blank.

The data were acquired using the Thermo Scientific^{TM} TraceFinder^{TM} 4.0 software. Data correction was performed by lock-mass corrected during the acquisition using GC column bleed siloxane masses. The mass results were processed by Thermo Scientific deconvolution software and identified by spectral matching using the National Institute of Standards and Technology (NIST). The percentage (%) of each content was calculated by the integrated area of the ion peaks of every compound in respect to that of the total ion peaks.

S1.5 Matrix-assisted laser Desorption Ionization Time of Flight Mass Spectrometry experiment

Matrix-assisted laser Desorption Ionization Time of Flight Mass Spectrometry (MALDI-TOF-MS) were recorded on AB Sciex 5800 for the sample PE-20. The test conditions refer to MALDI TOF mass spectra of poly-C_4H_6 synthesized by nickelocene based catalysts.[5] Samples were dissolved in tetrahydrofuran (THF) (5 mg / cm^{-3}) and mixed with matrix solution (2,5-dihydroxobenzoic acid (DHB) with CF_3COOAg, 1:1 and 5 mmol / cm^{-3}). Measurement was taken by using reflector mode in the range of 300-5000 m/z. It should be note that silver (Ag) has two isotopes (Ag^{107} and Ag^{109}) with approximately equal abundance. Hence, the signal of silver ion clusters (the mass difference in the set = 2) and samples (the mass difference in the set = 1) can be distinguished.

S1.6 Density functional theory calculation

Starting with crystal structure obtained from the Rietveld refinement result of in situ XRD experiment at 12.2 GPa, we employed the Density functional theory (DFT) calculation with Vienna Ab initio Simulation Package (VASP) code[6,7] to optimize the crystal structure at 0, 12 and 30 GPa. The projector-augmented plane-wave (PAW) method[8] was used with the local density approximation (LDA) exchange-correlation functional by Ceperley and Alder, as parameterized by Perdew and Zunger (CA-PZ).[9] Plane wave basis with an 540 eV energy cutoff was adopted while k-points solution was better than $2\pi\times0.05$ A^{-1}. Hydrogen transition reaction was investigated

via variable cell nudged elastic band (vc-NEB) method[10] with the help of USPEX code[11] at 0, 12 and 30 GPa, respectively. To better understand the C-H…π interaction, we took two adjacent molecules along x axis as a cluster from the optimized crystal structure and performed calculation in Gaussian software at a B3LYP/6-311G** level.[12] Multifunctional Wavefunction Analyzer (Multiwfn) software was used to further post processing.[13] Interaction region indicator (IRI) calculation was worked out to visualize the interaction between discussed molecules, which was defined as $IRI(r) = |\nabla\rho(r)|/[\rho(r)]^{\alpha}$.[14] α was set as 1.1 in this case. To measure the aromaticity for the six membered ring, a cluster consisted of two intermediate structures were similarly extracted from solid state structure. Nuclear independent chemical shift (NICS) for three position of the system was calculated in Gaussian (Figure S9).[15] Gauge-Independent Atomic Orbital (GIAO) method[16] was used to carried out magnetic shielding tensor. Non-covalent Interaction in all the calculations above was described by DFT-D3(BJ) correction.[17]

S2. Supplementary figures and tables

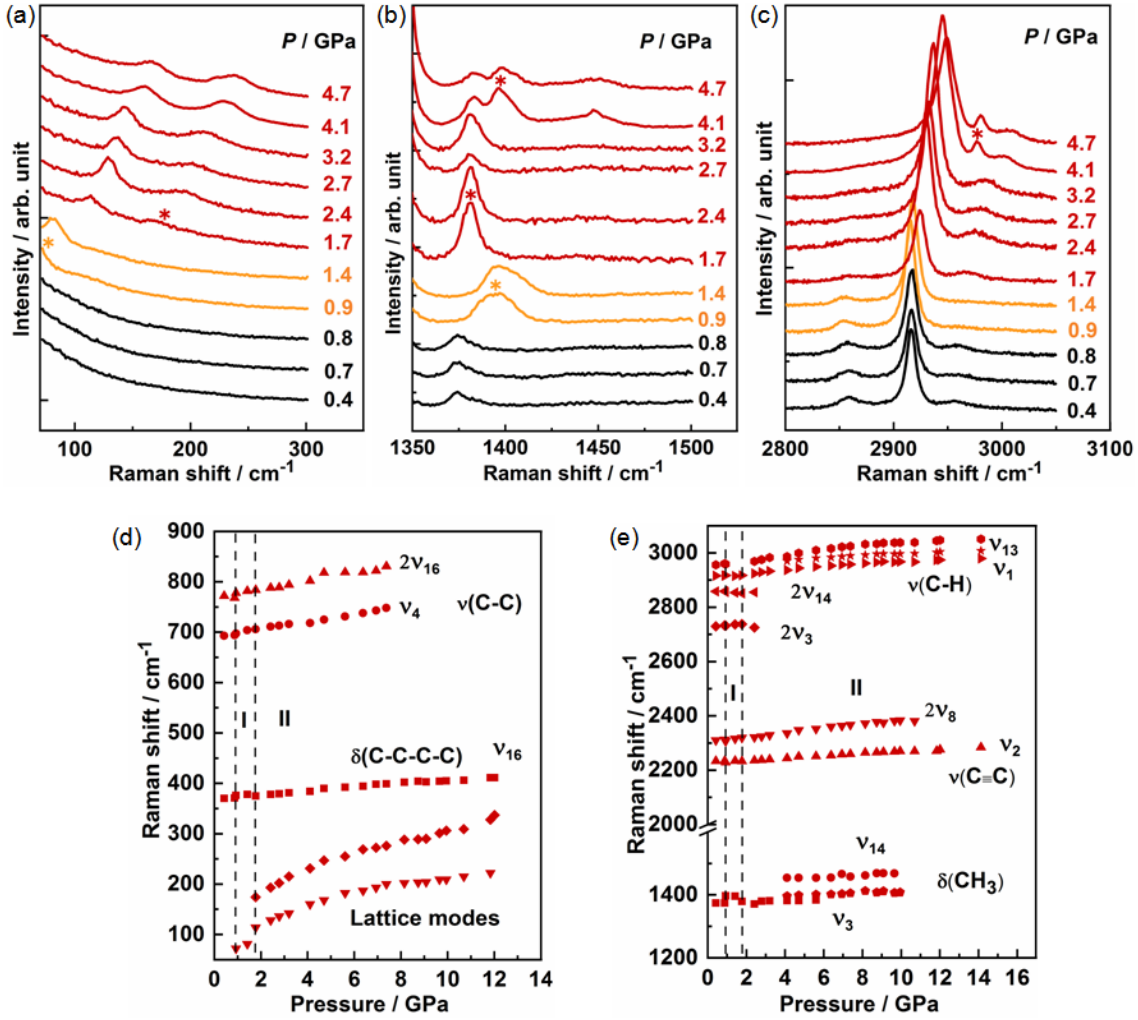

Figure S1. Selected Raman spectra of 2-butyne from 0.4 to 4.7 GPa in the range of (a) lattice modes region, (b) 1350-1500 cm^{-1} and (c) 2800-3050 cm^{-1}. The pressure dependence of Raman shift of 2-butyne in the range of (d) 60-900 cm^{-1} and (e) 1200-3100 cm^{-1}. I and II stand for phase I and II, respectively. The new peaks are asterisked.

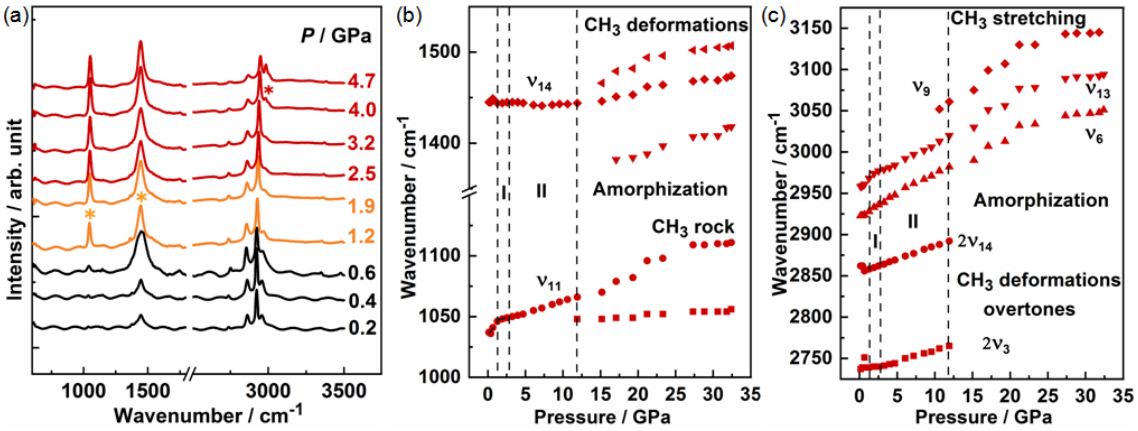

Figure S2. (a) Selected IR spectra of 2-butyne from 0.2 to 4.7 GPa; Pressure dependance of IR active modes in the range of (b) 1000-1550 cm^{-1} and (c) 2725-3175 cm^{-1}. I and II stand for phase I and II, respectively. The asterisks represent sudden changes in peak intensity or peak profile.

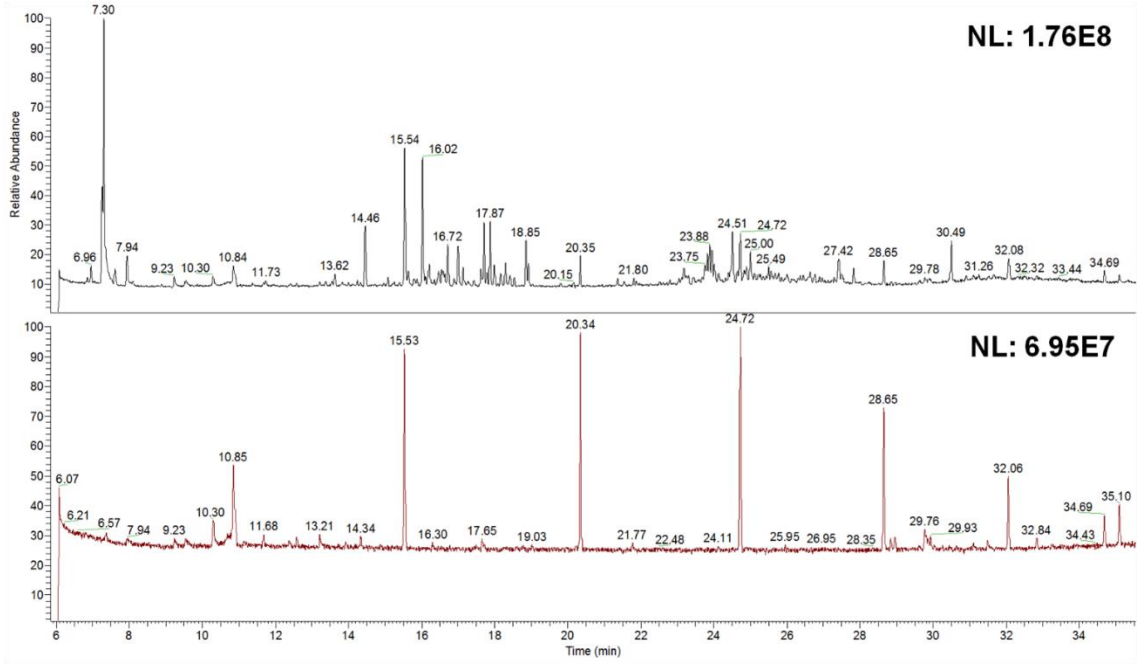

Figure S3. Gas Chromatography of soluble molecules from the sample PE-20. The black line is the chromatography of PE-20 sample dissolved in n-hexane and the red line is the standard chromatogram of n-hexane solvents. The mass spectra were collected with EI source.

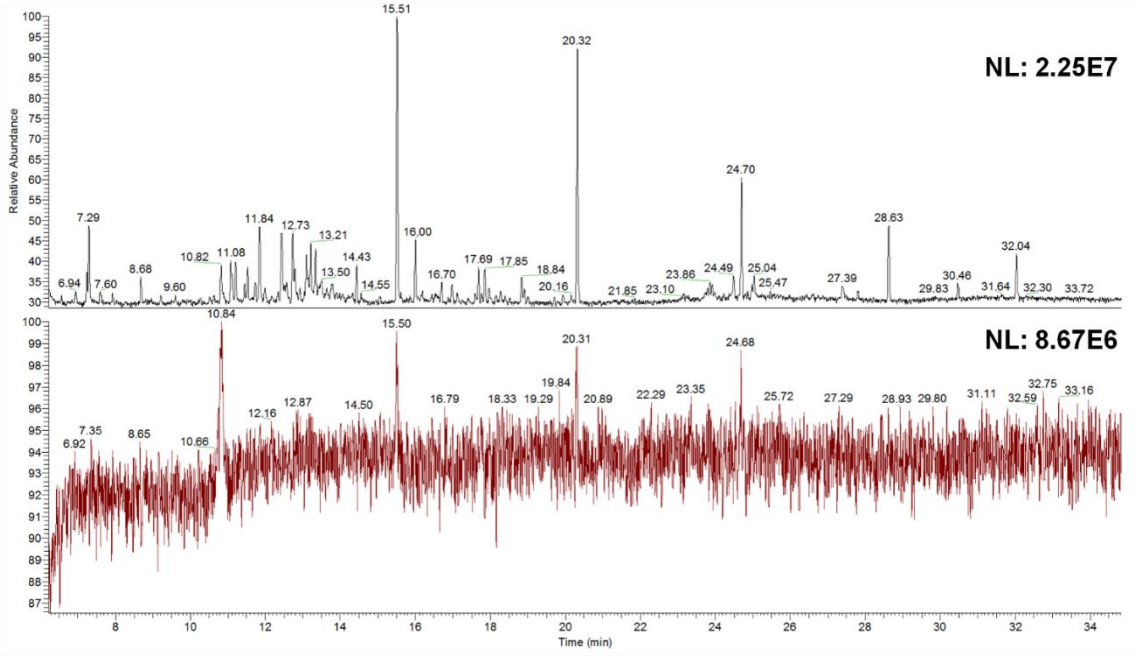

Figure S4. Gas Chromatography of soluble molecules from the sample PE-20. The black line is the chromatography of PE-20 sample dissolved in n-hexane and the red line is the standard chromatogram of n-hexane solvents. The mass spectra were collected with CI source.

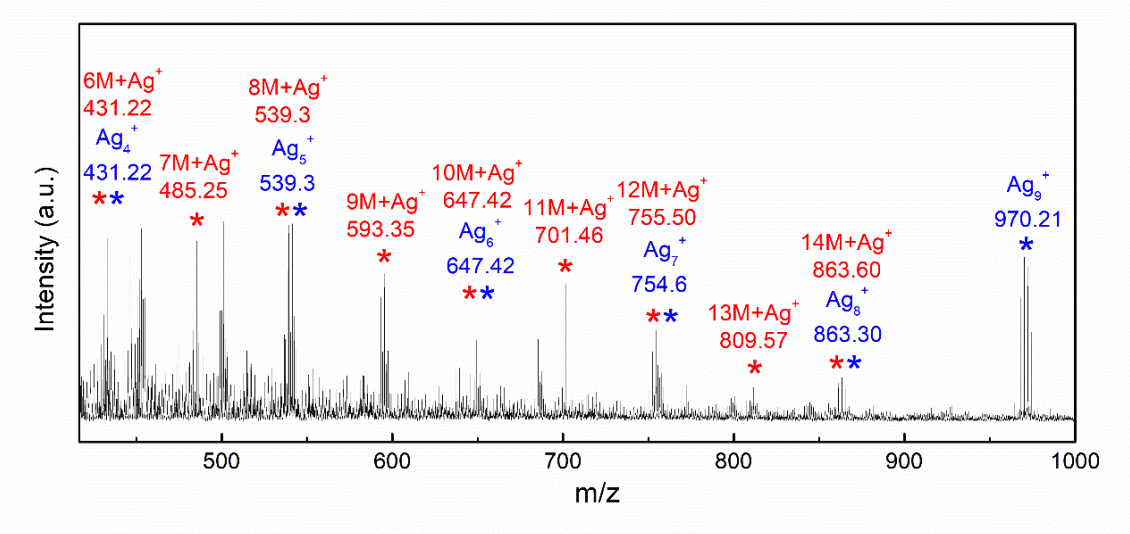

Figure S5. Matrix-assisted laser desorption ionization time of flight mass spectrum (MALDI-TOF-MS) of PE-20. The major peaks are ascribed to silver ion clusters and polymers with one silver ion. Polymers with degree of polymerization from 6 to 14 are detected.

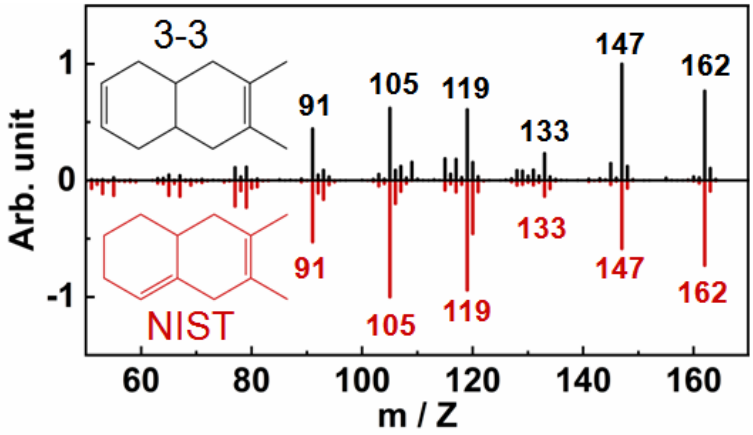

Figure S6. The mass spectra of 3-3 comparing with NIST spectra of 6,7-Dimethyl-1,2,3,5,8,8a-hexahydronaphthalene. The mass spectrum of 3-3 is not available in the database, so we use the mass spectra of a similar compound in NIST database for comparison.

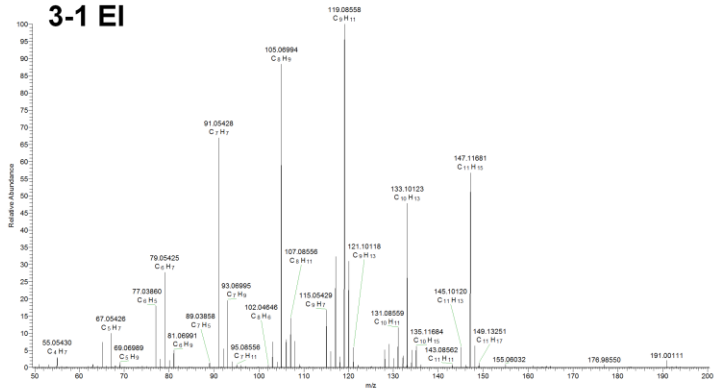
3-1 EI
Relative Abundance
m/z

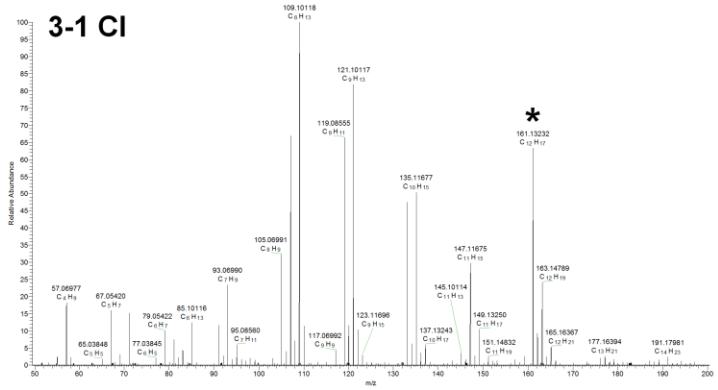
3-1 CI
Relative Abundance
m/z

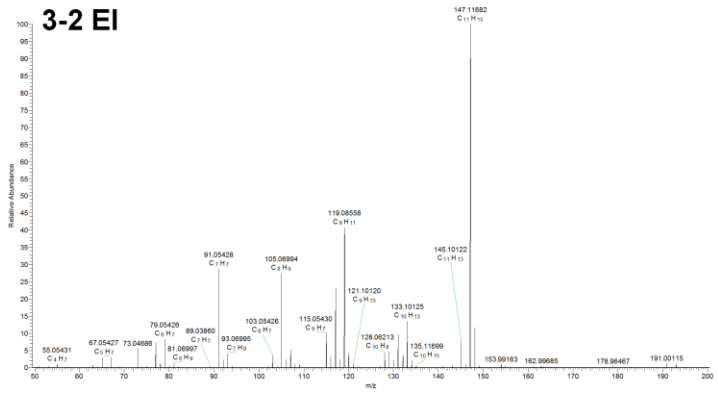
3-2 EI
Relative Abundance
m/z

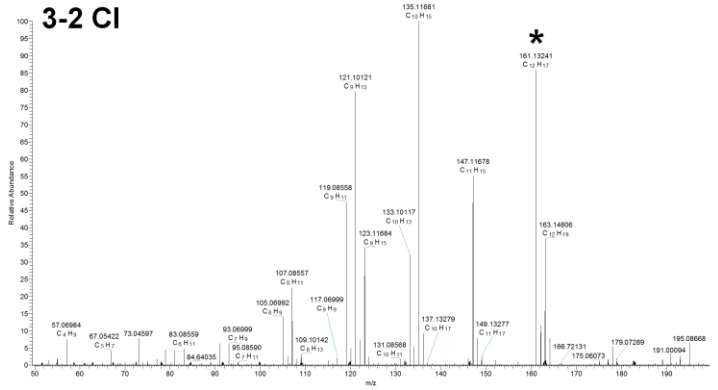
3-2 CI
Relative Abundance
m/z

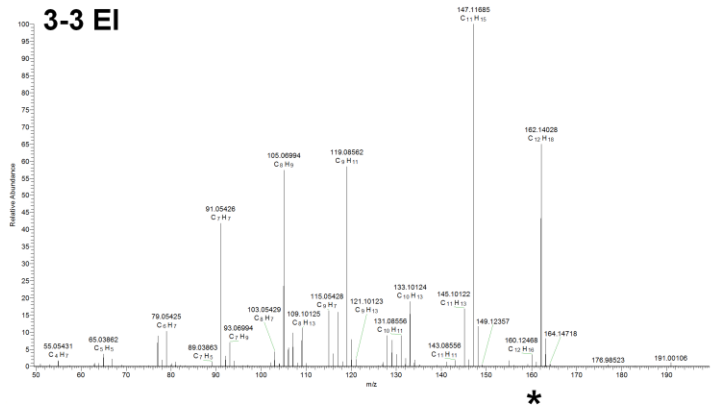
3-3 EI
Relative Abundance
m/z

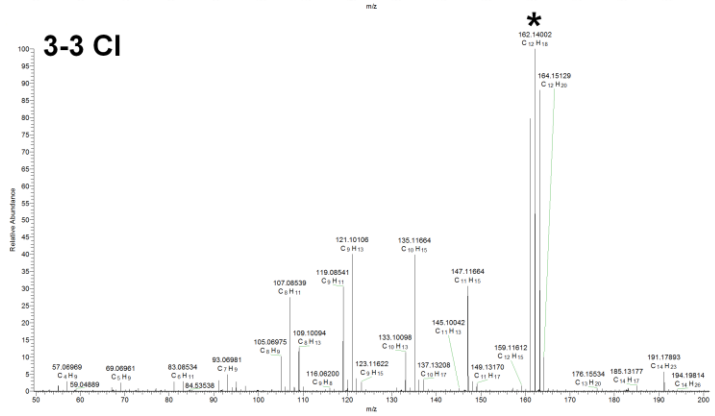
3-3 CI
Relative Abundance
m/z

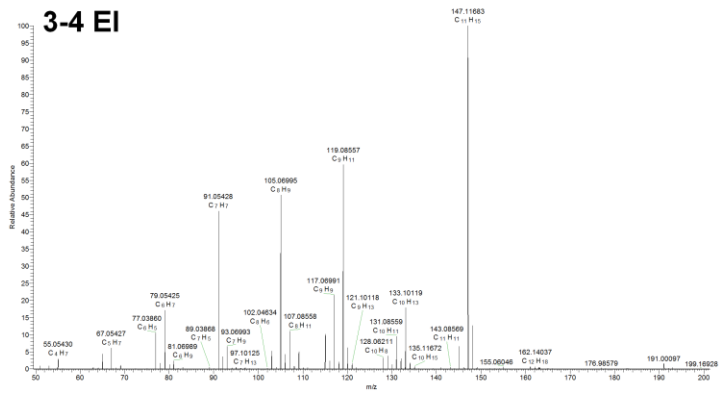
3-4 EI
Relative Abundance
m/z

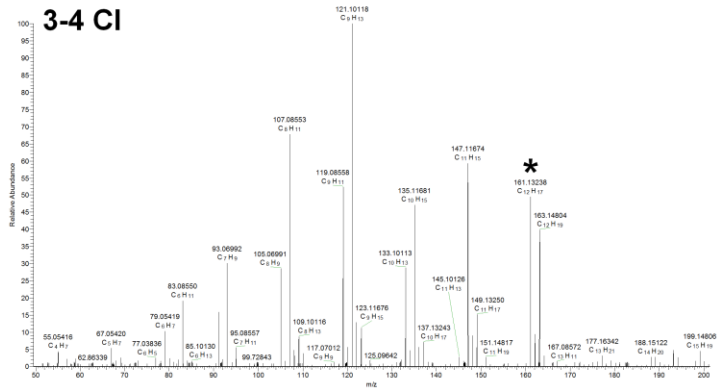
3-4 CI
Relative Abundance
m/z

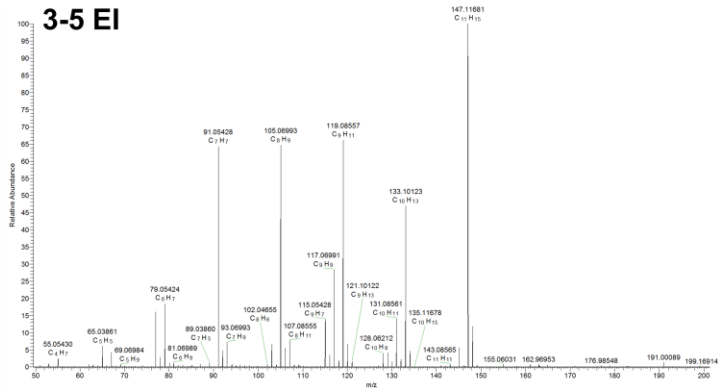
3-5 EI
Relative Abundance
m/z

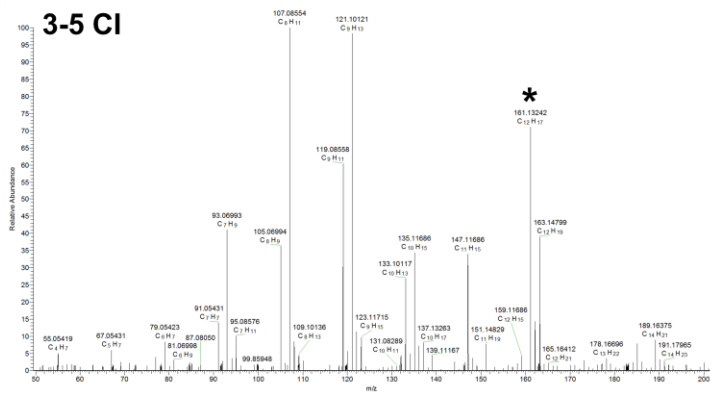
3-5 CI
*
Relative Abundance
m/z

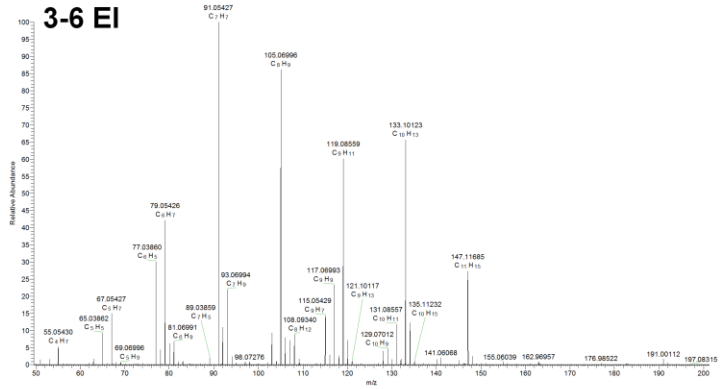
3-6 EI
Relative Abundance
m/z

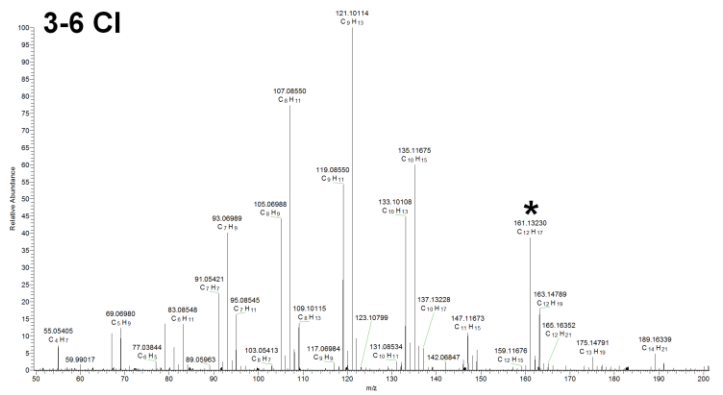
3-6 CI
*
Relative Abundance
m/z

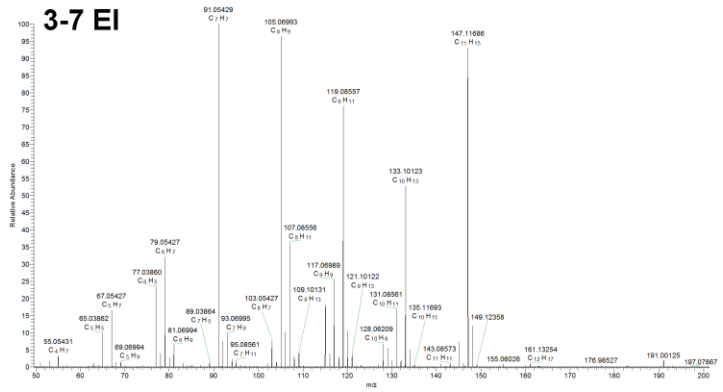
3-7 EI
Relative Abundance
m/z

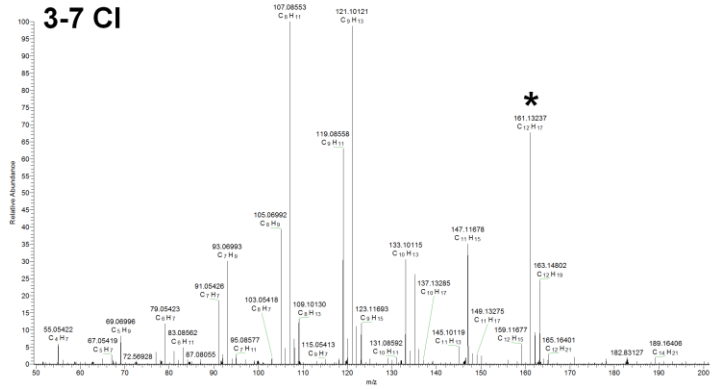
3-7 CI
*
Relative Abundance
m/z

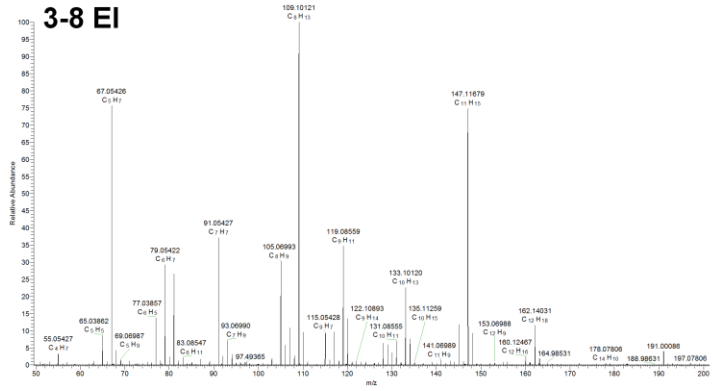
3-8 EI
Relative Abundance
m/z

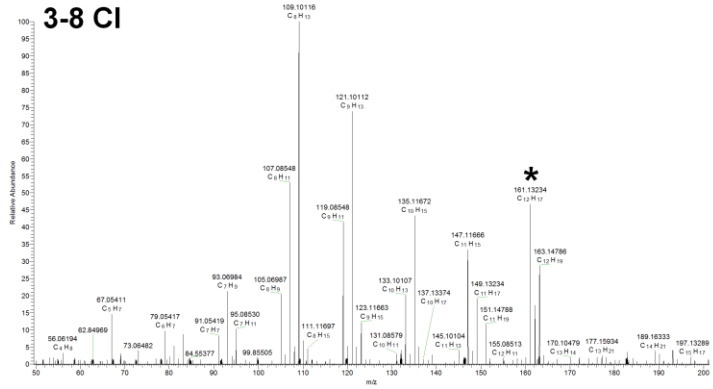
3-8 CI
*
Relative Abundance
m/z

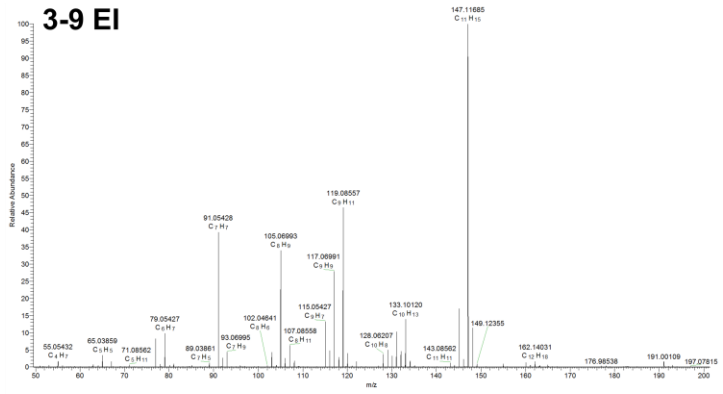
3-9 EI
Relative Abundance
m/z
147.11685
C11H15
119.08557
C9H11
91.05428
C7H7
105.06993
C8H9
117.06991
C9H9
133.10120
C10H13
115.05427
C9H7
149.12355
79.05427
C6H7
102.04641
C8H6
107.08558
C8H11
128.06207
C10H8
143.08562
C11H11
65.03859
C5H5
55.05432
C4H7
71.08562
C5H11
89.03861
C7H5
93.06995
C7H9
162.14031
C12H16
176.98538
191.00109
197.07815

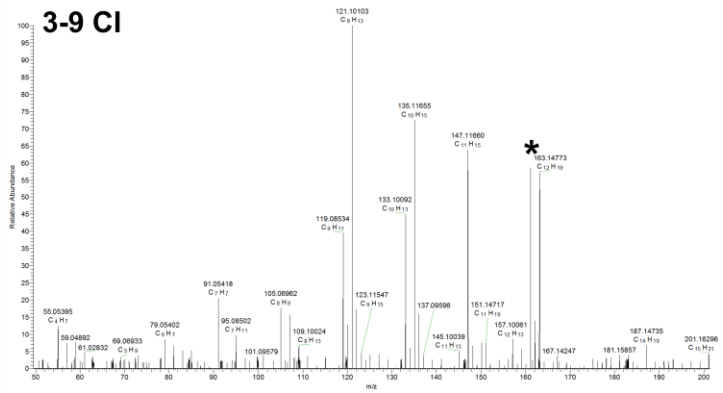
3-9 CI
Relative Abundance
m/z
121.10103
C9H13
135.11655
C10H15
147.11660
C11H15
*
163.14773
C12H19
133.10092
C10H13
119.08534
C9H11
91.05418
C7H7
105.06962
C8H9
123.11547
C9H15
137.09596
151.14717
C11H19
157.10061
C12H13
95.08502
C7H11
55.05395
C4H7
79.05402
C6H7
59.04892
69.06933
C5H9
61.02832
109.10024
C8H13
101.09579
145.10039
C11H13
167.14247
181.15857
187.14735
C14H19
201.16296
C15H21

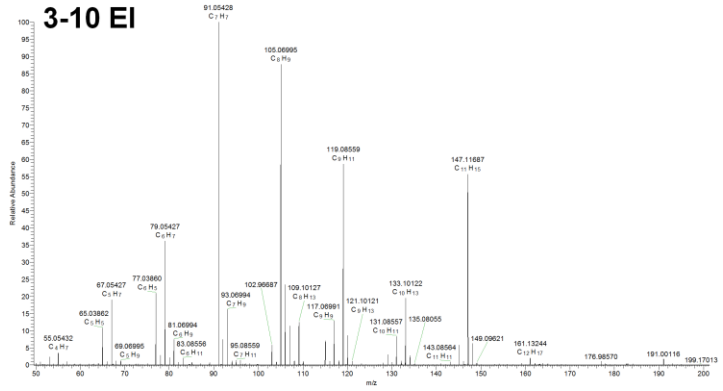
3-10 EI
Relative Abundance
m/z
91.05428
C7H7
105.06995
C8H9
119.08559
C9H11
147.11687
C11H15
79.05427
C6H7
77.03860
C6H5
67.05427
C5H7
65.03862
C5H5
93.06994
C7H9
102.96687
109.10127
C8H13
121.10121
C9H13
133.10122
C10H13
117.06991
C9H9
131.08557
C10H11
135.08055
81.06994
C6H9
55.05432
C4H7
69.06995
C5H9
83.08556
C6H11
95.08559
C7H11
143.08564
C11H11
149.09621
161.13244
C12H17
176.98570
191.00116
199.17013

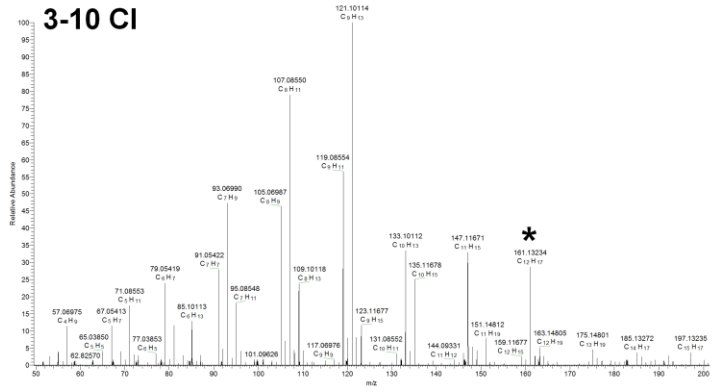
3-10 CI
Relative Abundance
m/z
121.10114
C9H13
107.08550
C8H11
119.08554
C9H11
93.06990
C7H9
105.06987
C8H9
133.10112
C10H13
147.11671
C11H15
*
161.13234
C12H17
91.05422
C7H7
79.05419
C6H7
135.11678
C10H15
109.10118
C8H13
71.08553
C5H11
95.08548
C7H11
57.06975
C4H9
67.05413
C5H7
85.10113
C6H13
123.11677
C9H15
65.03850
C5H5
77.03853
C6H5
62.82570
131.08552
C10H11
117.06976
C9H9
101.09626
144.09331
C11H12
151.14812
C11H19
159.11677
C12H15
163.14805
C12H19
175.14801
C13H19
185.13272
C14H17
197.13235
C15H17

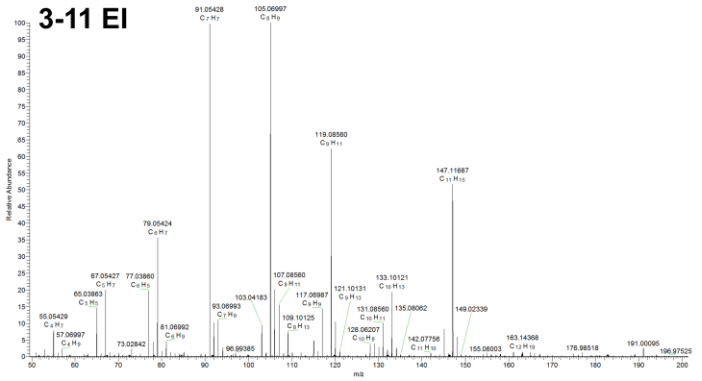
3-11 EI
Relative Abundance
m/z

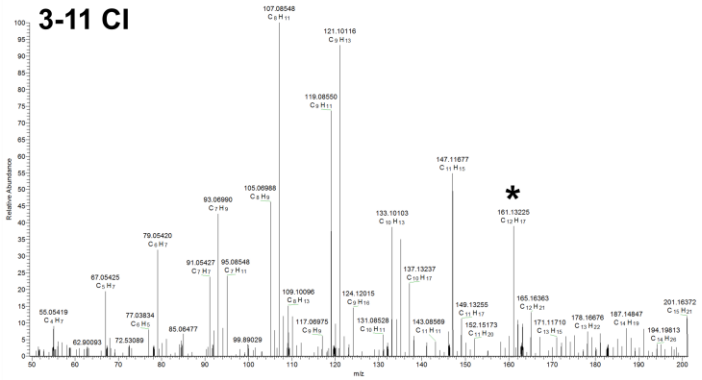
3-11 CI
Relative Abundance
m/z

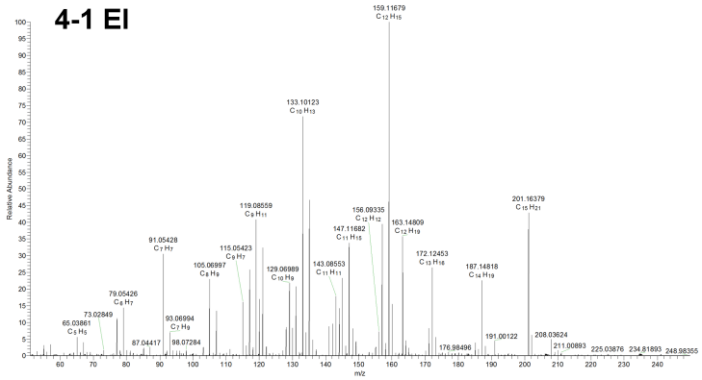
4-1 EI
Relative Abundance
m/z

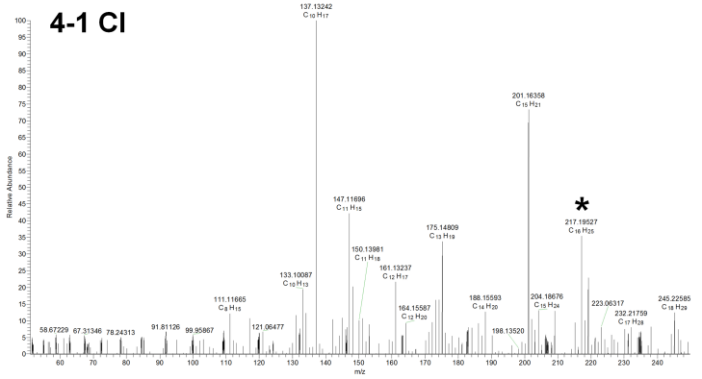
4-1 CI
Relative Abundance
m/z

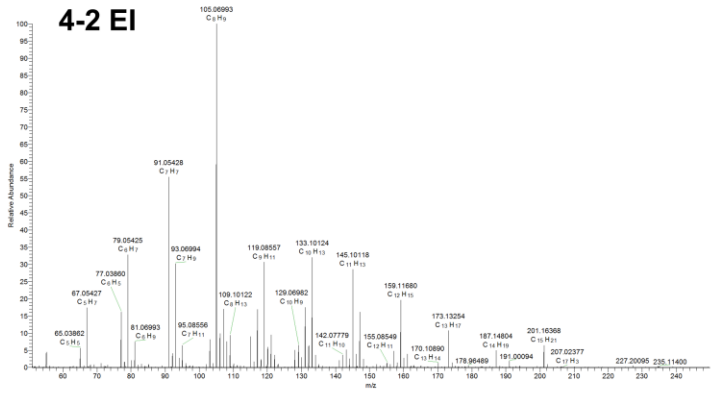
4-2 EI
Relative Abundance
m/z

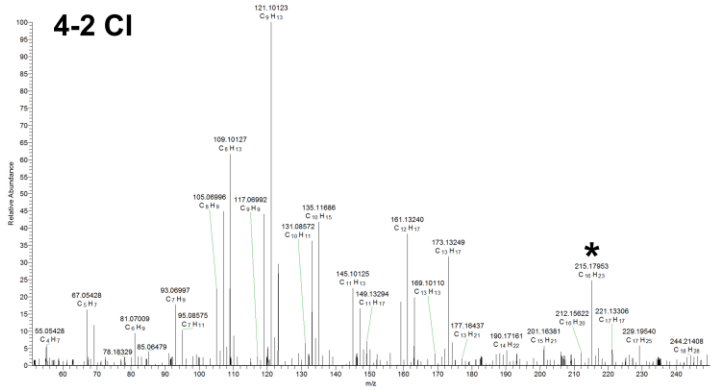
4-2 CI
Relative Abundance
m/z

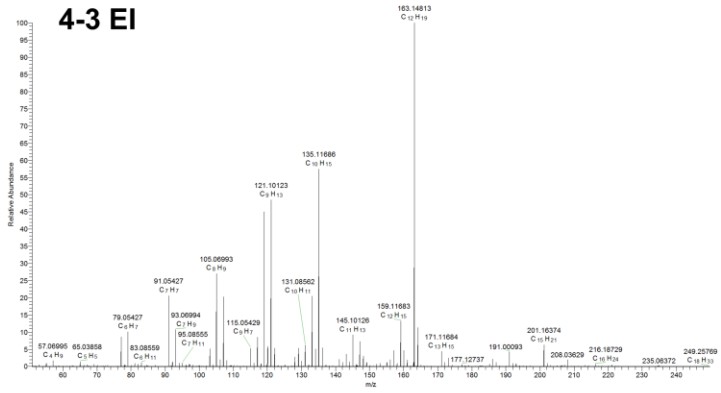
4-3 EI
Relative Abundance
m/z

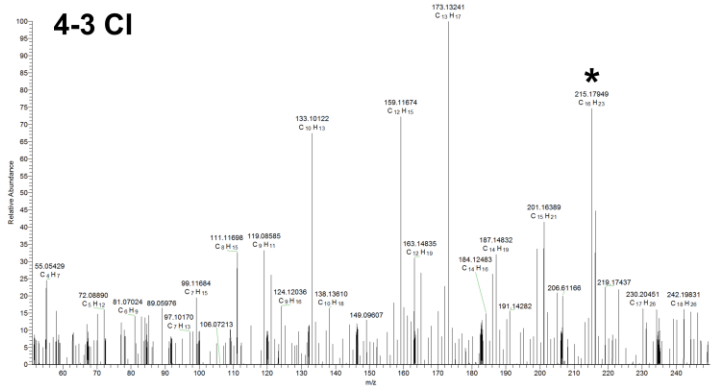
4-3 CI
Relative Abundance
m/z

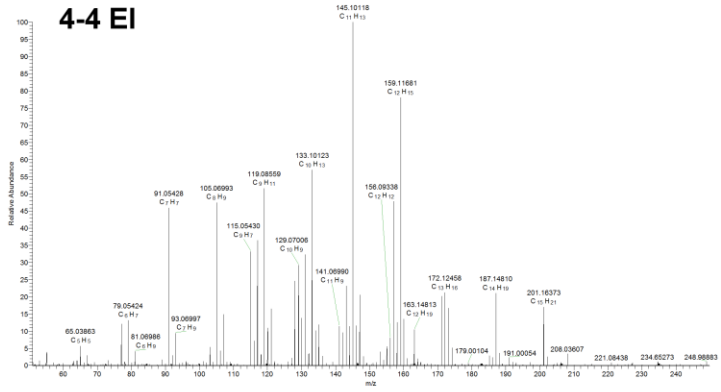
4-4 EI
Relative Abundance
m/z

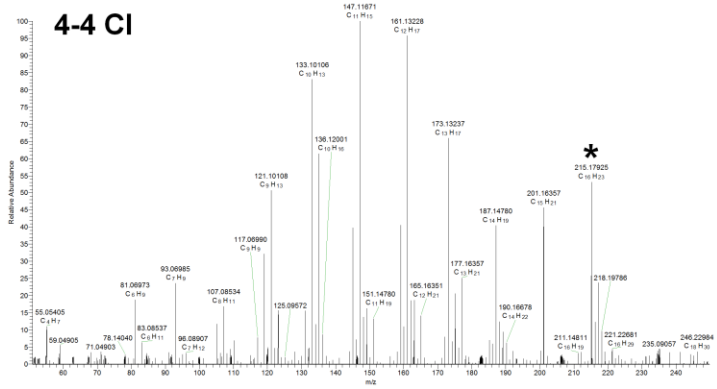
4-4 CI
Relative Abundance
m/z

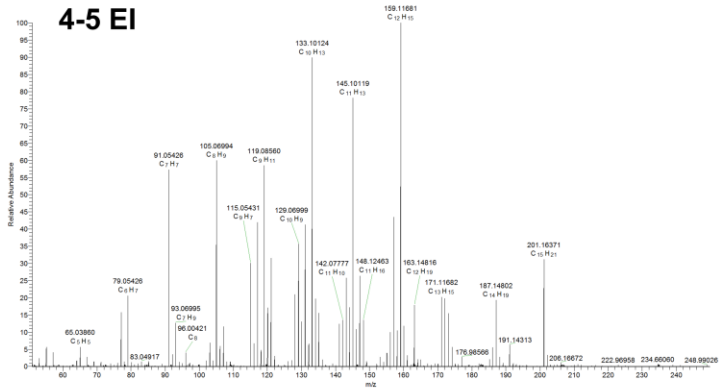
4-5 EI
Relative Abundance
m/z

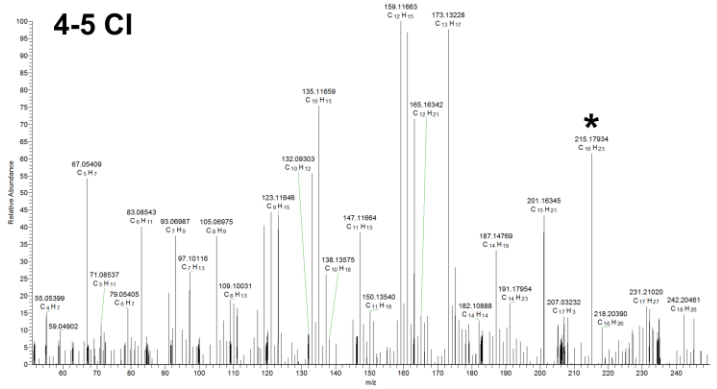
4-5 CI
Relative Abundance
m/z

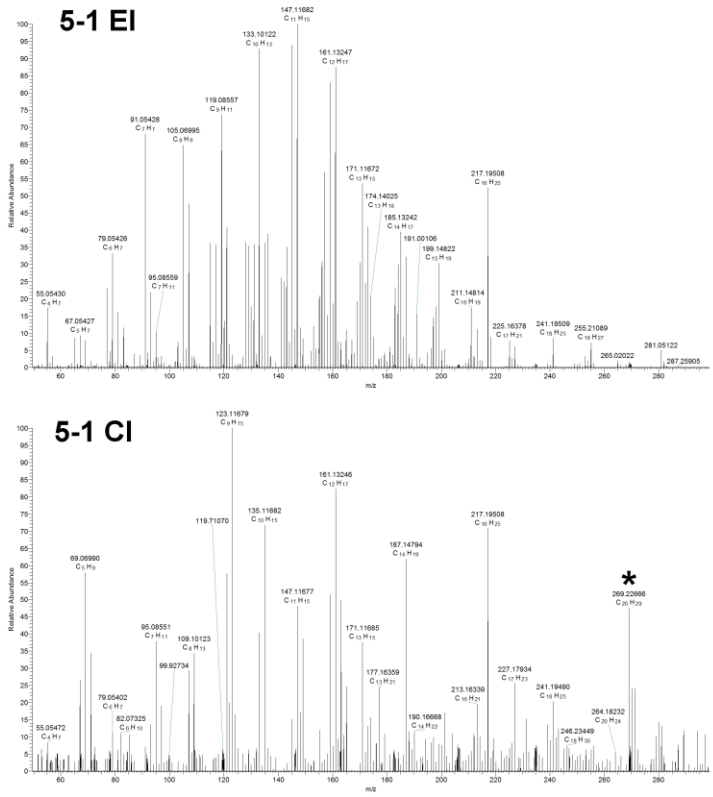

Figure S7. Selected high-resolution mass spectra of the sample PE-20 with electron ionization (EI) source and chemical ionization (CI) source. The asterisks stand for the molecular ion peaks of oligomers.

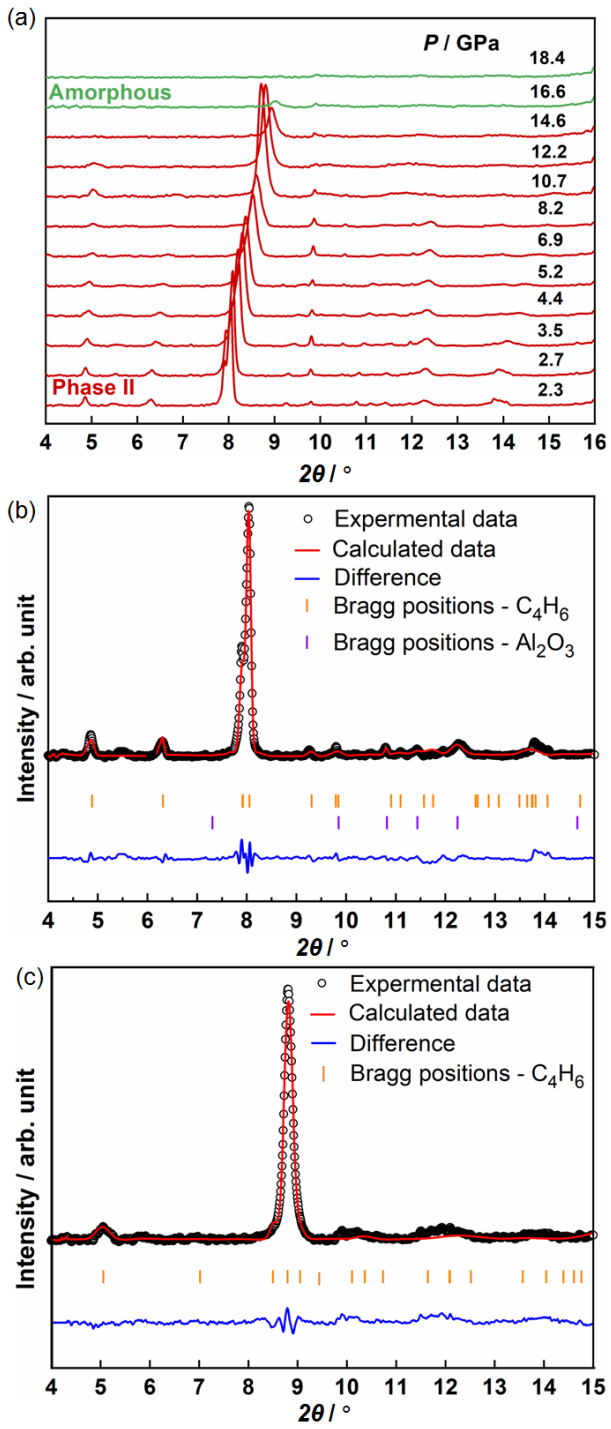

Figure S8. (a) In situ powder XRD patterns of 2-butyne from 2.3 to 18.4 GPa. Rietveld refinement plot of 2-butyne at (b) 2.3 GPa and (c) 12.2 GPa. The black circles, solid red line, solid blue line, and the bars represent the experimental data, simulated data, difference, and Bragg positions, respectively.

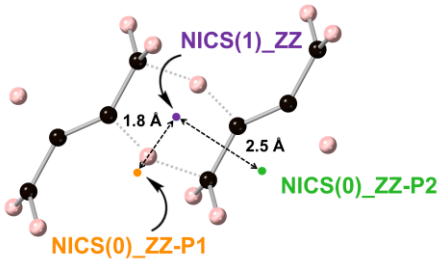

Figure S9. The NICS analysis of the 6-member ring intermediate state. The purple dot respresents the position at 1 Å above the center of the 6-member ring (NICS(1)_ZZ). The orange dot stands for the position at 1.8 Å away from the the ring center (NICS(0)_ZZ-P1), which is located along the extension line between the ring center and the hydrogen atom. The green dot represents the position at 2.5 Å away from the the ring center (NICS(0)_ZZ-P2).

Table S1. Assignment and frequencies of observed Raman and Infrared modes of 2-butyne.

Assignment	Raman (4.1 GPa)	Raman (Ref)[18,19]	Infrared (4.7 GPa)	Infrared (Ref) [18,19]	Vibration mode
R_x	162	183	-	-	-
R_y	230	258	-	-	-
δ(C-C-C-C)	384	396	-	-	ν_{16}
ν(C-C)	717	735	-	-	ν_4
2δ(C-C-C-C)	806	-	-	-	$2\nu_{16}$
ρ(CH_3 rock)	1047	1054	1051	1051	ν_{11}
ρ(CH_3 rock)	1031	1036	-	-	ν_{15}
ν(C-C)	-	-	-	1143	ν_8
δ(CH_3)	1396	1448	-		ν_3
δ(CH_3)	1453	-	1444	1445	ν_{14}
ν(C≡C)	2254	2256	-	-	ν_2
2ν(C-C)	2338	2356	-	-	$2\nu_8$
2δ(CH_3)	-	-	2746	2760	$2\nu_3$
2δ(CH_3)	-	-	2868	2864	$2\nu_{14}$
ν(C-H)	2945	2958	-	-	ν_1
ν(C-H)	-	-	2949	2944	ν_6
ν(C-H)	2977 3003	2989 3023	2984 -	2981 -	ν_{13}
ν(C-H)	-	-	3006	3003	ν_9

Table S2. Identification of the peaks in the total ion count (TIC) plot of sample PE-20.

Retention time (min)	Total ions of peaks in TIC	Percent %	Base ions (m/z)	m/z	Difference (Δppm)	Formula	Label
7.25	51572516	8.16%	91.0543	108.0934	0.444	C_8H_{12}	2-1
7.30	138353886	21.90%	93.0700	108.0934	0.444	C_8H_{12}	2-2
14.46	30763821	4.87%	119.0856	161.1324	-0.479	$C_{12}H_{17}^+$	3-1
15.54	63121951	9.99%	147.1168	161.1324	-0.479	$C_{12}H_{17}^+$	3-2
16.02	68080876	10.78%	147.1168	162.1403	-0.013	$C_{12}H_{18}$	3-3
16.72	22082344	3.50%	147.1168	162.1403	-0.013	$C_{12}H_{18}$	3-4
17.00	20917786	3.31%	147.1168	161.1324	-0.479	$C_{12}H_{17}^+$	3-5
17.71	33294476	5.27%	91.0543	161.1324	-0.479	$C_{12}H_{17}^+$	3-6
17.87	34819435	5.51%	91.0543	161.1325	0.023	$C_{12}H_{17}^+$	3-7
17.99	10247112	1.62%	109.1012	162.1403	-0.013	$C_{12}H_{18}$	3-8
18.29	12686992	2.01%	147.1168	162.1403	-0.013	$C_{12}H_{18}$	3-9
18.85	24601944	3.89%	91.0543	161.1325	0.023	$C_{12}H_{17}^+$	3-10
18.92	12351425	1.96%	105.0699	161.1325	0.023	$C_{12}H_{17}^+$	3-11
23.82	13508694	2.14%	159.1168	216.1874	0.148	$C_{16}H_{24}$	4-1
23.88	19328778	3.06%	105.0700	216.1874	0.148	$C_{16}H_{24}$	4-2
23.94	16208115	2.57%	163.1481	216.1873	0.048	$C_{16}H_{24}$	4-3
24.51	23759731	3.76%	91.0543	216.1871	-0.152	$C_{16}H_{24}$	4-4
25.00	14223509	2.25%	159.1168	216.1873	0.048	$C_{16}H_{24}$	4-5
30.49	21817072	3.45%	147.1167	270.2333	-0.902	$C_{20}H_{30}$	5-1

Table S3. Comparison of cell parameters between high-pressure phases and low-temperature phases.

	High-pressure phases (single crystal XRD results)		Low-temperature phases [20,21]	
	Phase I (1.2 GPa)	Phase II (1.8 GPa)	Phase I (220 K)	Phase II (5 K)
Space group	$P4_2/mnm$	$C2/m$	$P4_2/mnm$	$C2/m$
a (Å)	5.40(3)	5.22(5)	5.42	7.16
b (Å)	5.41(4)	7.189(8)	5.42	6.46
c (Å)	6.95(11)	5.25(5)	6.89	4.08
α°	90	90	90	90
β°	90	91(1)	90	101.05
γ°	90	90	90	90

Table S4. Selected Result of Rietveld refinement of the C_4H_6 structure under external pressure.

Pressure	2.3 GPa (Phase II)	12.2 GPa (Phase II)
Space group	$C2/m$	
a (Å)	5.046(4)	4.599(2)
b (Å)	6.287(3)	5.5283(4)
c (Å)	5.079(2)	4.982(3)
β°	91.18(9)	92.69(6)
Volume (Å^3)	161.11	126.54
Density (g/cm)	1.11	1.42
Z	2	
u(C)	0.0317 (fixed)	
C1	0.0884(8) 0 0.0808(6)	0.1085(2) 0 0.0721(2)
C2	0.3026(12) 0 0.2745(6)	0.3696(6) 0 0.2462(3)
R_p	0.0919	0.0896
R_{wp}	0.1269	0.1136

Table S5. NICS indexs in the 6-member ring intermediate state of hydrogen transfer.

Pressure / GPa	NICS(1)_ZZ / ppm	NICS(0)_ZZ-P1 / ppm	NICS(0)_ZZ-P2 / ppm
0	-15.69	4.50	2.36
12	-23.77	6.01	1.09
30	-24.26	6.46	6.83

S3. Supplemental references

(1) Mao, H.-k.; Xu, J.; Bell, P. M. Calibration of the ruby pressure gauge to 800 kbar under quasi-hydrostatic conditions, *J. Geophys. Res.* **1986**, *91*, 4673-4676.

(2) Prescher, C.; Prakapenka, V.B. DIOPTAS: a program for reduction of two-dimensional X-ray diffraction data and data exploration. *High Pressure Res.* **2015**, *35*, 285-288.

(3) Petricek, V.; Dusek, M.; Palatinus, L. Crystallographic computing system JANA2006: general features. *Z. Kristallogr.* **2014**, *229*, 345-352.

(4) Salmon, P. S.; Drewitt, J. W. E.; Whittaker, D. A. J.; Zeidler, A.; Wezka, K.; Bull, C. L.; Tucker, M. G. M.; Wilding, C.; Guthrie, M.; Marrocchelli, D. Density-driven structural transformations in network forming glasses: a high-pressure neutron diffraction study of GeO_2 glass up to 17.5 GPa. *J. Phys.: Condens. Matter* **2012**, *24*, 415102.

(5) Pasynkiewicz, S.; Oledzka, E.; Pietrzykowski, A. Polymerization of alkynes on nickelocene based catalysts: considerations on polymerization mechanism. *J. Mol. Catal. A: Chem.* **2004**, *224*, 117-124.

(6) Kresse, G.; Furthmüller, J. Efficiency of ab-initio total energy calculations for metals and semiconductors using a plane-wave basis set. *Comput. Mater. Sci.* **1996**, *6*, 15-50.

(7) Kresse, G.; Furthmüller, J. Efficient iterative schemes for *ab initio* total-energy calculations using a plane-wave basis set. *Phys. Rev. B* **1996**, *54*, 11169.

(8) Kresse, G.; Joubert, D. From ultrasoft pseudopotentials to the projector augmented-wave method. *Phys. Rev. B* **1999**. *59*, 1758-1775.

(9) Perdew, J. P.; Zunger, A. Self-interaction correction to density-functional approximations for many-electron systems. *Phys. Rev. B* **1981**, *23*, 5048-5079.

(10) Qian, G.-R.; Dong, X.; Zhou, X.-F.; Tian, Y.; Oganov, A. R.; Wang, H.-T. Variable cell nudged elastic band method for studying solid-solid structural phase transitions. *Comput. Phys. Commun.* **2013**, *184*, 2111-2118.

(11) Glass, C. W.; Oganov, A. R.; Hansen, N. USPEX-Evolutionary crystal structure prediction. *Comput. Phys. Commun.* **2006**, *175*, 713-720.

(12) Frisch, M. J.; Trucks, G. W.; Schlegel, H. B. et al. GAUSSIAN 09, Gaussian, Inc., Wallingford CT, 2009.

(13) Lu, T.; Chen, F. Multiwfn: A multifunctional wavefunction analyzer. *J. Comput. Chem.* **2012**, *33*, 580-592.

(14) Lu, T.; Chen, Q. Interaction region indicator: a simple real space function clearly revealing both chemical bonds and weak interactions. *Chemistry-Methods* **2021**, *1*, 231-239.

(15) Fallah-Bagher-Shaidaei, H.; Wannere, C. S.; Corminboeuf, C.; Puchta, R.; Schleyeret, P. v. R. Which NICS aromaticity index for planar π rings is best? *Org. Lett.* **2006**, *8*, 863-866.

(16) Wolinski, K.; Hinton, J. F.; Pulay, P. Efficient implementation of the gauge-independent atomic orbital method for NMR chemical shift calculations. *J. Am. Chem. Soc.* **1990**, *112*, 8251-8260.

(17) Grimme, S.; Ehrlich, S.; Goerigk, L. Effect of the damping function in dispersion corrected density functional theory. *J. Comput. Chem.* **2011**, *32*, 1456-1465.

(18) Baonza, V. G.; Montoro, O. R.; Taravillo, M.; Cáceres, M.; Núñez, J. Phase transitions and hindered rotation in dimethylacetylene at high pressures probed by Raman spectroscopy. *J. Chem. Phys.* **2004***, 121*, 11156-11162.

(19) Guan, J.; Daljeet, R.; Kieran, A.; Song, Y. Pressure-induced amorphization and reactivity of solid dimethyl acetylene probed by in situ FTIR and Raman spectroscopy. *J. Phys.: Condes. Matter* **2018**, *30*, 224004.

(20) Pionataro, E.; Post, B. The crystal structure of dimethyl acetylene at -50 °C. *J. Acta Crysta.* **1955**, *8*, 672-674.

(21) Ibberson, R. M.; Prager, M. The *ab initio* crystal-structure determination of perdeuterodimethylacetylene by high-resolution neutron powder diffraction. *Acta Crystallogr., Sect. B: Struct. Sci.* **1995**, *B51*, 71-76.